Application of modern analog technique to marine Antarctic diatoms: Reconstruction of maximum sea-ice extent at the Last Glacial Maximum

Xavier Crosta, Jean-Jacques Pichon, Burckle Lloyd

PALEOCEANOGRAPHY, VOL. 13, NO. 3, PAGES284-297, JUNE 1998

Application of modern analog technique to marine Antarctic diatoms: Reconstruction of maximum sea-ice extent at the Last Glacial Maximum

X. Crosta and J.-J. Pichon

Département de Géologie et Océanographie, UMR-CNRS 5805, Université de Bordeaux I, Talence Cedex, France

L. H. Burckle

Lamont-Doherty Earth Observatory of Columbia University, Palisades, New York

Abstract. Modern analog technique (MAT) applied to Antarctic diatoms is a new approach for quantitative sea-ice paleoreconstructions in the Southern Ocean. In a first step we show that MAT is a better approach than the Imbrie and Kipp Method to reconstruct the modern sea-ice pattern. We then use this approach to reconstruct sea-ice presence in number of months per year during the last glacial maximum (LGM). At this time, sea-ice presence was greater than today, leading to a shorter diatom growing season. The maximum sea-ice extent, inferred from quantitative values of sea-ice presence, was located 5-8° north of its actual position, leading to double the surface of modern winter sea ice. This greater sea-ice extent may have played a significant role on atmospheric and surface oceanic circulations and therefore on southern mid-latitude and high-latitude climates. It may also have reduced the amount of heat, moisture, and CO_2 from the ocean to the atmosphere, thus participating in the lowering of atmospheric CO2 during the LGM.

1. Introduction

During their transfer to the seafloor, diatom frustules are affected by processes such as remineralization and zooplankton grazing [*Sakshaug and Holm-Hansen*, 1984; *Von Bodungen et al.*, 1985; *Gersonde and Wefer*, 1987]. Alteration of the frustules at the water/surface sediment can also be caused by preferential dissolution, resuspension, and lateral transport by bottom currents [*Ledford-Hoffman et al.*, 1986; *Crosta et al.*, 1997]. Despite the alteration of the original assemblage, earlier works on diatom distributions in surface sediments have shown that the surviving fossil assemblages are related to surface water hydrology [*Truesdale and Kellogg*, 1979; *DeFelice and Wise*, 1981; *Burckle*, 1984; *Leventer*, 1992; *Pichon et al.*, 1992a; *Zielinski and Gersonde*, 1997].

The annual sea ice is a favorable environment for sympagic diatoms [*Horner*, 1985]. It acts as a substrate on which ice diatoms can grow and reach higher biomass than in the underlying water column. During the spring/summer decay, ice algae are released in the nutrient-rich and stable surface water layer near the sea-ice edge as an inoculum for summer blooms [*Hasle*, 1969; *Wilson et al.*, 1986]. A succession of the diatom assemblages from ice algae blooms (primarily pennate diatoms) to phytoplankton blooms (primarily centric diatoms) may be the result of the decreasing influence of the sea-ice environment associated with the summer sea-ice retreat. Hence it is that diatom fossil assemblages are related to sea-ice cover and that they can be used to reconstruct sea-ice extent and seasonality in the past using statistical methods such as the Imbrie and Kipp Method (IKM) [*Imbrie and Kipp*, 1971] and the modern analog technique (MAT) [*Hutson*, 1980].

Changes in climate occur over a wide range of timescales and space scales and involve interactions within a planetary system that includes ice sheets, the atmosphere, the surface of the land, and the entire world ocean [*Climate: Long-Range Investigation, Mapping, Prediction* (CLIMAP), 1976]. General circulation models dealing with some of these aspects are only beginning to reveal the role of each field [*Watkins and Simmonds*, 1995; *Godfred-Spenning and Simmonds*, 1996]. The Southern Ocean is a major component of the global climate system, in particular for its role in deep water formation and the oceanic carbon cycle. In this region, questions of distribution of the winter and summer sea-ice cover during the last glacial maximum (LGM) are important in climate modeling because of its role on albedo, heat exchange between ocean and atmosphere, and oceanic mixing.

Early works dealing with seasonal sea-ice extent during the LGM were qualitative and used lithlogical proxies, inferred sea-ice-rafted debris records, sedimentation rates, and faunal changes from deep-sea cores [*CLIMAP*, 1981; *Hays et al.*, 1976; *Cooke and Hays*, 1982, *Burckle*, 1984]. In this study, using a new diatom modern database, we test the ability of MAT to reconstruct Southern Ocean sea-ice presence, expressed as number of months per year, for the present. Then, we use this technique to quantitatively reconstruct this parameter during the LGM in order to provide new data to general circulation models (GCMs).

2. Material and Methodology

2.1. Modern Data Set

Diatom taxonomy has been calibrated with researchers from the Alfred-Wegener Institute of Bremerhaven, Germany. The

Paper number 98PA00339.
0883-8305/98/98PA-00339$12.00

modern database was developed from the data set already used by *Pichon et al.* [1992a, 1992b] and is composed of 195 surface sediment samples. The most important differences with their work are (1) no artificially dissolved samples were introduced in this study as we wanted to use a totally natural modern data set; (2) new diatom species or species group were added such as Chaetoceros resting spores; and (3) diatom species such as *Eucampia antarctica*, which is an ubiquist species, and the two silicoflagelates genera were removed. Samples were selected (1) on natural criteria such as the depth of the sample in the core (maximum 4 cm for cores with high rates of sedimentation), the total number of diatoms counted in the samples (more than 250), and the relative abundance of reworked species (less than 2%); and (2) on statistical criteria given by the *Q*-mode factor analysis (samples displaying communality lower than 0.7 are not representative of the actual sedimentation) [*Imbrie and Kipp*, 1971; *Le*, 1992].

The new modern database covers the Atlantic and Indian sectors of the Southern Ocean from 40°S to the Antarctic Continent plus the Ross Sea and the western part of the Antartic Peninsula (Table 1 and Figure 1). No samples were available from the Pacific sector of the southern Ocean.

2.2. LGM Data Set

Diatom analysis was performed on 106 samples dated around 18,000 years B.P. Of those, 89 are CLIMAP points [*CLIMAP*, 1976, 1981]; the 17 others samples are from R/V *Marion Dufresnes* cruises. Dates of the LGM are provided by oxygen isotopic and radiolarian stratigraphy for the CLIMAP samples [*CLIMAP*, 1981], and by *Cycladophora davisiana* biostratigraphy [*Hays et al.*, 1976] for the French samples or biogenic silica measurements [*Bareille et al.*, 1990] for the samples: KR 88-22, KR 88-27 and KR 88-29. This data set covers the Atlantic sector of the Southern Ocean between 40° and 60°S, the Indian sector between 35°S and the Antarctic Continent, and the eastern Pacific sector between 50° and 65°S (Table 2). Only 12 samples were available from the Pacific sector of the Southern Ocean.

2.3. Sample Preparation and Counting

Slides were prepared using the settling technique fully described by *Rathburn et al.* [1997] and fixed in Naphrax. Diatom counts follow *Schrader and Gersonde* [1978] and *Laws* [1983]. Generally, a minimum of 300 diatom valves were counted in each sample using a Zeiss photomicroscope at a magnification of x1000. Diatoms were identified to species or species groups level, and the relative abundance of each species was determined.

2.4. Modern Environment Data

The source of recent sea surface temperature (SST) data is the World Ocean Atlas [*Levitus*, 1994]. This atlas is built as a grid in which each square represents 1° of latitude and 1° of longitude. SST in one square is interpolated from the SST values of all the control points present in this square. The extraction program was kindly provided by R. Sieger from the Alfred-Wegener Institute of Bremerhaven, Germany. SSTs were extracted for summer (February) and winter (August) for surface water (0 m).

The source of modern sea-ice data are charts from the *Naval Oceanography Command Detachment* [1985]. This atlas contains sea-ice summaries derived from 521 weekly sea-ice analyses performed between 1973 and 1982. The groups of charts are composed over a semimonthly period centered on the first and the fifteenth of each month. To obtain quantitative values of recent sea ice for each sample, a map with their position was placed over the analyzed charts, and the total number of half-month presence of sea ice was calculated.

2.5. Statistical Techniques

2.5.1. IKM. The IKM is a robust working technique as demonstrated by its wide usage. It has been successfully applied to foraminifera to estimate past SSTs in the Atlantic Ocean [*Imbrie and Kipp*, 1971; *McIntyre et al.*, 1989; *Mix et al.*, 1986], in the Indian Ocean [*Howard and Prell*, 1992], and to marine diatoms in the Southern Ocean [*Pichon et al.*, 1987, 1992a].

The procedure starts with a *Q*-mode factor analysis (principal component analysis and varimax rotation of the selected principal rotation). The objective of the *Q*-mode factor analysis is to describe an observed sample by a linear combination of several factors. Factor loadings describe the importance of the factors in accounting for the variance of the samples. The sum of the square of the factor loadings in a sample is the communality which describes the amount of variance accounted for by the factors. The next step is to fit an empirical equation between factor loadings and values of the parameter using a curvilinear regression. To estimate values (modern or past), factor loadings derived from the calibration are introduced into the empirical equation [*Le and Shackleton*, 1994].

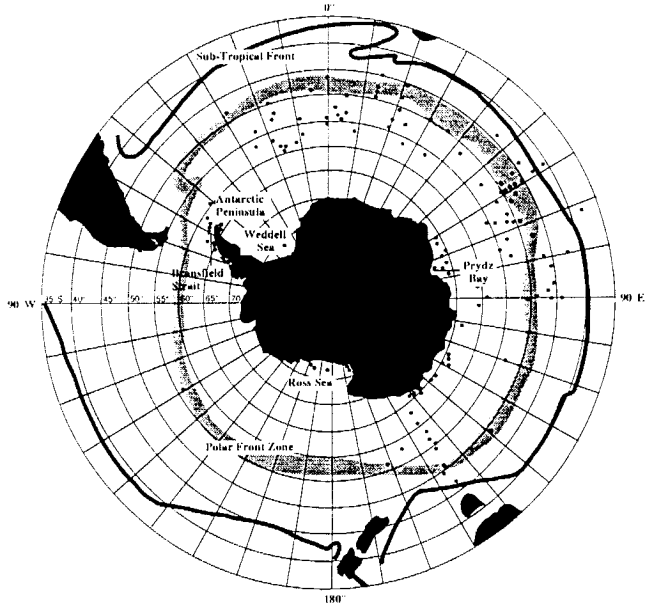

Figure 1. Geographic and hydrologic details of the study area and locations of the surface sediment samples used in the modern database (dots). The location of the oceanographic fronts is given according to *Tchernia* [1978].

Table 1. Locations and Water Depths of Surface Samples Used in the Modern Database

Core	Level, cm	Latitude, °S	Longitude	Depth, m	Core	Level, cm	Latitude, °S	Longitude	Depth, m
RC11-118	Top	37°48'	71°32'E	4354	KR87-07	Top	62°21'	57°58'W	2810
RC11-119	Top	40°18'	74°34'E	3709	PCDF82-35	Top	62°22'	57°22'W	1484
KTB31	Top	40°59'	57°59'E	5077	PCDF82-71	Top	62°38'	59°32'W	1350
KTB34	Top	41°59'	58°01'E	4800	PCDF82-47	Top	62°55'	58°24'W	723
MDBX94-01	Top	42°30'	79°25'E	2895	PCDF82-69	Top	63°00'	59°38'W	916
KTB29	Top	43°00'	58°01'E	4765	KR87-06	Top	63°04'	63°04'W	630
RC8-40	Top	43°45'	46°05'E	2250	PCDF82-61	Top	63°17'	59°20'W	728
KTB26	Top	43°58'	55°58'E	4527	KR88-23	Top	63°18'	117°16'E	3292
MDBX94-06	Top	44°39'	90°04'E	3709	KR88-15	Top	63°18'	141°55'E	3880
IO1176-91	Top	44°57'	15°03'E	4649	PCDF82-60	Top	63°23'	59°34'W	673
KTB25	Top	45°01'	57°57'E	4680	KR88-27	Top	63°39'	101°09'E	1210
IO1277-2	Top	45°03'	22°28'E	4806	PCDF82-51	Top	63°43'	60°03'W	560
MDBX94-02	Top	45°35'	86°31'E	3205	PCDF82-197	Top	63°43'	57°14'W	750
KR88-02	Top	45°45'	82°56'E	3480	KR88-24	Top	63°45'	116°45'E	2600
KTB21	Top	45°58'	55°59'E	4195	PCDF82-167	Top	63°52'	56°37'W	448
KTB22	Top	45°59'	55°59'E	4260	PCDF82-1	Top	63°57'	56°22'W	430
KR88-03	Top	46°04'	90°07'E	3400	PCDF82-93	Top	64°04'	61°20'W	690
MDBX94-03	Top	46°28'	88°03'E	3559	PCDF82-174	Top	64°10'	56°49'W	288
KR88-01	Top	46°41'	79°29'E	2925	PCDF82-20	Top	64°14'	55°54'W	381
RC11-80	Tw2-3	46°45'	00°03'W	3656	KR88-25	Top	64°18'	115°42'E	2232
IO1176-88	Top	46°57'	14°18'E	5106	PCDF82-102	Top	64°19'	61°53'W	540
KTB20	Top	47°00'	58°01'E	4550	KR88-19	Top	64°34'	135°38'E	2930
KR88-07	Top	47°09'	145°48'E	2890	PCDF82-134	Top	64°34'	62°39'W	793
RC11-98	Top	47°39'	61°29'E	4650	PCDF82-112	Top	64°36'	61°38'W	564
MD84-569	Top	47°39'	73°23'E	1720	PCDF82-127	Top	64°39'	62°07'W	443
IO1678-80	Top	47°57'	13°01'W	3120	KR88-22	Top	64°40'	119°30'E	3140
IO1277-4	Top	47°59'	21°35'E	3150	PCDF82-136	Top	64°45'	62°45'W	452
KTB18	Top	48°00'	57°59'E	4245	KR88-21	Top	64°49'	126°43'E	2250
IO1176-86	Top	48°02'	13°49'E	4338	PCDF82-140	Top	64°50'	62°38'W	392
IO1678-112	Top	48°09'	27°59'W	3250	PCDF82-142	Top	63°51'	62°26'W	541
MDBX94-05	Top	48°48'	89°32'E	4036	KR88-20	Top	64°56'	129°00'E	1670
MD84-529	Top	48°54'	62°00'E	2600	PCDF82-155	Top	65°01'	63°16'W	437
RC11-79	Tw2-3	49°00'	04°36'W	3100	MD84-533	Top	65°09'	78°21'E	3363
KTB12	Top	49°00'	57°59'E	4390	KR88-18	Top	65°45'	138°12'E	615
KR88-06	Top	49°01'	128°46'E	3850	MD84-530	Top	66°07'	73°59'E	2412
KTB01	Top	49°06'	57°01'E	1235	MD84-532	Top	66°07'	76°46'E	2700
KR88-08	Top	49°16'	148°48'E	3885	KR88-17	Top	66°12'	140°30'E	180
IO1176-82	Top	49°31	13°11'E	4100	AA93-7/105GR	Top	66°34'	62°45'E	1882
V29-87	Top	49°34'	30°01'E	4550	AA93-7/73GR	Top	66°37'	69°24'E	1435
RC15-91	TW3-4	49°55'	15°34'S	3775	AA93-7/106GR	Top	66°52'	63°10'E	434
KR 88-04	Top	49°55'	100°05'E	3350	DF86-119TC	Top	66°57'	69°52'W	600
V16-60	Top	49°59'	36°45'E	4575	MD84-531	Top	66°58'	75°25'E	365
KTB14	Top	50°00'	57°59'E	4610	AA93-7/24GR	Top	66°59'	76°19'E	330
MD84-521	Top	50°08'	06°47'E	4150	GC5	Top	67°03'	69°05'E	376
MDBX94-04	Top	50°22'	90°16'E	3460	GC33	Top	67°11'	68°30'E	320
IO1277-8	Top	50°32'	20°53'E	4492	AA93-7/23GR	Top	67°21'	76°35'E	318
KR88-09	Top	50°36'	147°09'E	4350	AA93-7/78GR	Top	67°31'	68°12'E	460
MD84-563	Top	50°43'	68°09'E	1720	DF86-106TC	Top	67°49'	67°59'W	520
MD80-304	Top	51°04'	67°44'E	1950	DF86-103TC	Tw2-3	67°53'	67°37'W	370
MD84-562	Top	51°55'	68°14'E	3553	DF86-110TC	Top	67°55'	68°25'W	700
MD24-KK63	Top	51°56'	42°53'E	2550	DF86-111TC	Top	67°56'	68°25'W	815
IO1678-84	Top	51°57'	14°25'W	3952	DF86-102TC	Tw1-2	67°58'	67°37'W	238
KTB08	Top	51°59'	61°07'E	4710	AA93-7/21GR	Top	68°01'	76°33'E	460
MD82-422	Top	52°34'	02°14'E	3750	DF86-101TC	Top	68°04'	67°40'W	258

Table 1. (continued)

Core	Level, cm	Latitude, °S	Longitude	Depth, m	Core	Level, cm	Latitude, °S	Longitude	Depth, m
RC11-95	Tw2-3	52°48'	54°05'E	3150	DF86-118TC	Tw2-3	68°05'	69°17'W	582
KR88-05	Top	52°57'	109°55'E	3510	AA93-7/60GR	Top	68°06'	72°15'E	788
MD24-KK37	Top	52°58'	23°46'E	2905	DF 86-100TC	Tw1-2	68°08'	67°42'W	406
RC11-77	Top	53°03'	16°27'W	4098	AA93-7/42GR	Top	68°11'	75°52'E	695
MD84-561	Top	53°05'	71°36'E	1754	DF86-94TC	Top	68°16'	68°33'W	641
MD24-KK35	Top	53°06'	19°25'E	2725	AA93-7/9GR	Top	68°26'	77°48'E	173
MD84-557	Top	53°20'	75°48'E	1080	AA93-7/59GR	Top	68°27'	72°01'E	509
IO1176-55	Top	53°23'	06°40'E	2926	DF86-91TC	Top	68°29'	70°06'W	1079
RC13-263	Top	53°48'	08°13'W	3389	AA93-7/39GR	Top	68°33'	74°25'E	775
MD80-301	Top	54°00'	66°50'E	3750	AA93-7/38GR	Top	68°37'	74°31'E	667
IO1678-64	Top	54°01'	24°12'W	4515	AA93-7/19GR	Top	68°39'	76°43'E	775
IO1277-12	Top	54°01'	19°48'E	3178	AA93-7/13GR	Top	68°40'	77°16'E	538
MD82-424	Top	54°06'	00°21'W	2350	AA93-7/12GR	Top	68°42'	77°31'E	707
KR88-10	Top	54°11'	144°48'E	2785	AA93-7/18GR	Top	68°43'	76°45'E	820
MD24-KK02	Top	54°13'	03°31'E	1522	AA93-7/17GR	Top	68°47'	76°48'	798
MD24-KK32	Top	54°30'	03°48'E	2020	AA93-7/15GR	Top	68°49'	77°10'E	760
KR88-11	Top	54°55'	144°04'E	2880	AA93-7/14GR	Top	68°55'	76°54'E	700
MD84-552	Top	54°55'	73°50'E	1780	AA93-7/GR158	Top	68°55'	76°37'E	700
RC8-46	Top	55°20	65°28'E	2761	AA93-7/41GR	Top	68°57'	73°34'E	792
MD82-425	Top	55°35'	00°43'W	1940	AA93-7/37GR	Top	68°58'	75°11'E	775
KR88-12	Top	56°24'	145°17'E	3020	AA93-7/43GR	Top	69°14'	76°06'E	548
ELT33-21	Tw1-2	56°26'	119°48'W	2240	DFBC83-27II	Top	75°42'	170°39'E	322
ELT36-38	Tw3-4	56°28	161°46'E	2258	DFBC83-28II	Top	75°51'	169°18'E	485
RC11-91	Tw3-4	56°34'	34°11'E	5150	DFBC83-29II	Top	76°01'	167°12'E	622
RC11-90	Tw2-3	56°38'	25°43'E	5334	DFBC83-30II	Top	76°05'	166°42'E	668
V14-53	Top	56°43'	24°31'W	7906	DFBC83-1II	Top	76°10'	168°58'E	540
IO1678-89	Top	57°04'	18°32'W	4285	DFBC83-40II	Top	76°21'	167°12'E	732
IO1176-65	Top	57°13'	08°12'E	5483	DFBC83-5II	Top	76°30'	166°00'E	640
MD82-428	Top	57°19'	07°59'W	3750	DFBC83-23II	Top	76°31'	170°05'E	860
ELT36-33	Top	57°46'	154°55'	1877	DFBC83-2II	Top	76°37'	164°21'E	540
MD82-430	Top	57°52'	10°40'W	3863	DFBC83-42III	Top	76°38'	166°03'W	420
KR88-13	Top	57°57'	144°35'E	3740	DFBC83-41III	Top	76°40'	164°01'W	516
MD82-445	Top	58°18'	16°02'W	5750	DFBC83-21II	Top	76°41'	167°49'E	768
MD82-432	Top	58°39'	14°55'W	4150	DFBC83-43III	Top	76°43'	176°19'W	541
MD82-443	Top	58°47'	15°26'W	5650	DFBC83-20II	Top	76°47'	166°41'E	750
MD82-434	Top	58°52'	16°39'W	3640	DFBC83-10II	Top	76°57'	166°20'E	878
MD82-433	Top	58°53'	15°12'W	4750	DFBC83-9II	Top	77°05'	166°31'E	915
KR88-31	Top	59°00'	89°24'E	4595	DFBC83-1III	Top	77°10'	169°07'E	930
KR87-10	Top	59°40'	51°17'W	2820	DFBC83-8II	Top	77°10'	165°48'E	871
MD84-540	Top	60°44'	86°23'	3964	DFBC83-19III	Top	77°18'	158°43'W	677
KR87-08	Top	60°55'	56°26'W	2150	P1010	Top	77°20'	35°00'W	476
KR88-30	Top	61°00'	93°12'E	4300	DFBC83-7II	Top	77°21'	165°53'E	880
KR88-14	Top	61°17'	144°26'E	4200	DFBC83-6II	Top	77°30'	165°48'E	823
PCDF82-34	Top	62°18'	57°37'W	1979					

RC, piston core from Robert Conrad; KTB, multicore from Marion Dufresne; MDBX and KR, Marion Dufresne box cores; IO, piston core from Island Orcadas; MD, kullenberg from Marion Dufresne; V, Vema; PC and DF, piston cores from U.S. Coast Guard Glacier; AA, piston core from Aurora Australis; GC, grab core from Franklin; ELT, Eltanin trigger cores; and DFBC, deep-freeze box cores.

Because the phytoplankton population of the Southern Ocean is dominated by a few species present in all the core tops whatever the surface water hydrology, IKM needs to increase the statistical weight of background species sensitive to local surface hydrology [*Pichon et al.*, 1987]. Therefore the IKM based on Antarctic diatoms uses a ranking system in four classes rather than relative percentages (Table 3). Relative abundances to 0.3% belong to the rank 0 to minimize the effect of contamination by specimens from another biogeographic zone during slide preparation.

2.5.2. MAT. MAT compares the floral assemblage from each sample to a subset of modern floral core-top analogs. It

Table 2. Locations and Depths in the Core of the Last Glacial Maximum (LGM) Horizon

Core	Latitude, °S	Longitude	Depth, m	LGM depth, cm	Core	Latitude, °S	Longitude	Depth, m	LGM depth, cm
ELT49-37	51°42'S	100°03'E	3540	58-59	RC13-261	56°07'S	08°41'W	4221	81-82
ELT50-8	50°56'	104°54'E	3226	158-159	RC13-263	53°48'	08°13'W	3389	180-181
ELT50-11	55°57'	104°57'E	3923	99-100	RC13-271	51°59'	04°31'E	3634	948-949
ELT50-13	60°00'	105°00'E	4209	39-40	RC13-273	55°05'	11°35'E	4967	60-61
ELT49-17	46°17'	90°15'E	3502	39-40	RC13-275	50°43'	13°26'E	1984	59-60
ELT49-10	59°01'	110°08'E	4371	61-62	RC13-276	47°42'	14°42'E	5015	40-41
ELT50-17	62°00'	120°03'E	4081	90-91	RC14-11	38°00'	54°11'E	3268	80-81
ELT49-19	43°53'	90°06'E	3304	98-99	RC14-12	38°45'	59°18'E	5271	100-101
ELT49-23	47°08'	95°05'E	3257	38-39	RC15-93	46°06'	13°14'W	2714	98-99
ELT49-24	47°59'	95°02'E	3213	39-40	RC17-61	52°12'	54°28'E	3947	261-262
ELT49-25	49°23'	94°50'E	3336	83-84	RC17-63	45°39'	48°17'E	2947	241-242
ELT49-29	57°06'	94°57'E	4237	38-39	RC12-241	43°28'	57°39'W	3499	70-71
ELT49-33	57°46'	100°02'E	4040	39-40	RC 12-289	47°54'	23°41'W	4484	61-62
ELT45-64	52°29'	114°05'E	3825	41-42	RC12-291	42°35'	17°48'W	3508	80-81
ELT45-69	48°51'	114°37'E	3413	41-42	RC13-251	42°31'	11°40'E	4341	18-19
ELT45-71	48°02'	114°29'E	3660	38-39	RC13-253	46°36'	07°37'E	2494	40-41
ELT45-74	47°33'	114°26'E	3806	41-42	RC13-254	48°34'	05°08'E	3636	60-61
ELT45-79	45°03'	114°22'E	4099	41-42	RC13-255	50°35'	02°54'E	3332	140-141
ELT49-6	51°00'	109°59'E	3326	98-99	RC11-78	50°52'	09°52'W	3115	178-179
ELT49-7	53°02'	110°03'E	3592	59-60	RC11-80	46°45'	00°03'W	3656	81-82
ELT49-8	55°04'	110°01'E	3692	102-103	RC11-83	41°36'	09°43'E	4718	338-339
ELT35-15	52°56'	116°59'W	3766	200-201	RC11-91	56°34'	34°11'E	5373	20-21
ELT36-36	60°23'	157°32'E	2818	102-103	RC11-93	56°18'	51°58'E	5373	540-541
ELT39-13	45°01'	125°59'E	4538	62-63	RC11-94	54°29'	53°03'E	4303	500-501
ELT39-18	48°01'	126°05'E	4615	39-40	RC11-96	50°28'	59°35'E	4839	100-101
ELT39-21	48°52'	126°01'E	4078	82-83	RC11-97	50°19'	61°12'E	4638	22-23
ELT45-29	44°53'	106°31'E	3821	41-42	RC11-118	37°48'	71°32'E	4354	39-40
ELT45-35	53°30'	111°20'E	3920	161-162	RC11-119	40°18'	74°34'E	3709	39-40
ELT45-63	53°26'	114°15'E	3920	141-142	RC11-120	43°31'	79°52'E	3193	79-80
ELT11-4	57°48'	115°12'W	4776	14-15	RC8-39	42°53'	42°21'E	4330	91-92
ELT11-12	65°52'	115°05'W	4721	18-19	RC8-43	48°41	57°22'E	4319	41-42
ELT14-6	57°01'	160°06'W	4520	112-113	RC8-46	55°20'	65°28'E	2761	19-20
ELT15-4	59°01'	99°46'W	4914	59-60	RC9-139	47°46'	123°06'E	4158	51-52
ELT15-12	58°41'	108°48'W	4575	31-32	RC11-71	49°08'	37°25'W	5537	400-401
ELT17-9	63°05'	135°07'W	4851	160-161	RC11-77	53°03'	16°27'W	4098	200-201
ELT21-20	60°15'	120°10'W	4703	161-162	MD82-424	54°05'	00°21'W	2350	260-261
ELT15-6	59°58'	101°19'W	4910	27-28	MD84-551	55°00'	73°16'E	1504	160-161
V14-57	57°34'	17°06'W	4978	200-201	MD73-026	44°59'	53°17'E	3429	253-254
V16-65	45°00'	45°46'E	1618	40-41	MD84-527	43°29'	51°19'E	3262	300-301
V16-115	55°41'	141°17'E	3147	100-101	MD24-KK63	51°56'	42°53'E	2550	320-321
V18-110	53°35'	44°42'W	2610	30-31	MD88-770	46°01'	96°28'E	3290	110-111
V22-108	43°11'	03°15'W	4171	100-101	MD84-529	48°54'	61°32'E	2600	40-41
V24-203	36°59'	59°59'E	4997	179-180	MD88-769	46°04'	90°06'E	3420	110-111
V29-84	43°51'	27°36'E	5451	120-121	MD88-772	50°01'	104°54'E	3240	140-141
V29-86	49°34'	30°01'E	5614	181-182	MD88-773	52°54'	109°52'	2460	430-431
V29-87	49°06'	27°23'E	5314	21-22	MD88-787	56°23'	145°18'E	3020	250-251
V29-89	45°44'	25°39'E	5945	120-121	MD84-552	54°55'	73°50'E	1780	170-171
V29-90	43°42'	25°44'E	5148	58-59	MD80-304	51°04'	67°44'E	1950	240-241
ELT11-1	54°54'	114°42'W	3477	42-43	MD82-434	58°52'	16°39'W	3640	140-141
ELT11-2	56°03'	115°04'W	3111	138-139	KR88-29	62°30'	95°53'E	3790	16-17
ELT11-3	56°54'	115°15'W	4026	60-61	KR88-27	63°39'	101°09'E	1210	20-21
RC13-256	53°11'	00°21'W	2525	400-401	KR88-22	64°40'	119°30'E	3140	45-46

ELT, Eltanin; V, Vema; RC, Robert Conrad; and MD and KR, Marion Dufresne.

calculates a dissimilarity coefficient which measures the difference between the assemblage of the sample and the assemblage of the analog. Calculation of the dissimilarity coefficient is based on the squared chord distance [*Prell*, 1985].

This approach has several advantages over other statistical estimation techniques. (1) It can be applied directly to relative species abundances and therefore does not require any ranking or factor analysis which may smooth or generalize the data. (2) The location of the analogs provides geographic information which may help to reconstruct past environmental conditions. (3) Rare species with low relative abundances are as important as dominant species. (4) Estimates are only weighted averages of the analog parameter values. The MAT gives a standard error for each estimate (SEE) instead of a mean standard deviation on the whole range of estimate for the IKM. Finally, (5) any new reliable sample can be added to the modern database and can contribute to the result of any subject sample [*Pflaumann et al.*, 1996] without changing the entire equation as in IKM.

On the other hand the MAT approach has several disadvantages. (1) It needs a wider distribution of surface

Table 3. Conversion of Relative Percentages Into Abundance Ranks for Each Species

Taxa/Rank	Rank 0	Rank 1	Rank 2	Rank 3
Actinocyclus actinochilus	0.3	1	2.493	2.987
Azpetia tabularis	0.3	1	6.247	10.494
Azpetia tab. var egregius	0.3	1	2.027	2.053
Chaetoceros resting spore gp.	0.3	1	47.981	93.961
Fragilariopsis curta	0.3	1	34.162	66.324
Fragilariopsis cylindrus	0.3	1	2.478	2.956
Fragilariopsis doliolus	0.3	1	20.8	39.601
Fragilariopsis kerguelensis	0.3	1	43.336	84.672
Fragilariopsis obliquecostata	0.3	1	6.698	11.397
Fragilariopsis rhombica	0.3	1	2.951	3.901
Fragilariopsis ritscherii	0.3	1	2.51	3.021
Fragilariopsis separanda	0.3	1	4.855	7.709
Fragilariopsis sublinearis	0.3	1	4.078	6.155
Hemidiscus cuneiformis	0.3	1	3.926	5.853
Porosira glacialis	0.3	1	4.269	6.537
Porosira pseudodenticulata	0.3	1	2.132	2.263
Rhizosolenia ant. var semis.	0.3	1	3.898	5.796
Rhizosolenia styliformis	0.3	1	3.268	4.536
Roperia tessalata	0.3	1	4.177	6.354
Stellarima microtrias	0.3	1	2.651	3.302
Thalassionama nitz. var lanc.	0.3	1	3.109	4.218
Thalassionama nitz. var parva	0.3	1	3.31	4.62
Thalassionema nitzschioides	0.3	1	2.99	3.979
Thalassiosira antarctica gp.	0.3	1	17.191	32.383
Thalassiosira eccentrica	0.3	1	2.515	3.03
Thalassiosira gracilis	0.3	1	7.633	13.266
Thalassiosira lentiginosa	0.3	1	21.165	40.33
Thalassiosira oestrupii	0.3	1	5.989	9.979
Thalassiosira oest. var vanr.	0.3	1	2.418	2.836
Thalassiosira oliverana	0.3	1	3.188	4.375
Thalassiosira tumida	0.3	1	2.061	2.123
Thalassiothrix spp.	0.3	1	2.692	3.384
Trichotoxon reinboldii	0.3	1	2.894	3.789

sediment samples than the IKM to provide reliable analogs of any subject sample. (2) It is very sensitive to the number of analogs chosen for the estimated reconstruction and to the maximal acceptable value of the dissimilarity coefficient. The choice of this maximal value is empirical. We have chosen to use five analogs and a maximal dissimilarity coefficient of 0.25 because they give the best results on the modern model (lowest residuals and standard deviations).

3. Results

3.1. Reconstruction of the Modern Model

A total of 110 diatom taxa or taxa groups have been identified in the 195 periantarctic surface sediments of the modern data set. Relative abundances of 42 taxa or taxa groups displaying more than 1% of the total assemblage have been plotted against February sea surface temperatures (SSTsfeb) (Figure 2) and sea-ice presence in number of months per year (Figure 3). Of those, 33 species or species groups have been selected for IKM and MAT reconstructions because (1) they represent more than 2% of the total diatom assemblages and (2) their higher relative abundances in modern sediments constrain particuliar SSTsfeb and sea-ice presence (Figures 2 and 3, underlined species names).

3.1.1. IKM: Results of factor analysis. The *Q*-mode factor analysis of the relative abundances of the 33 selected diatom species in the 195 surface sediment samples resolved four varimax factors accounting for 87% of the variance (Table 4). All factors are related to surface parameters (SST or sea-ice cover). The addition of a fifth factor accounts for 1.5% of the total variance and is unrelated to any discernable biogeographic, physical, or chemical influence. We chose to label this version of the transfer function IKM195/33/4; future references will use this label for more comprehension.

Factor 1 accounts for 35.5% of the total variance (Table 4) and is dominated by three species, *Fragilariopsis curta*, *Fragilariopsis obliquecostata* and *Fragilariopsis sublinearis* (Table 5) which are species especially well adapted to the sea-ice habitat [*Hasle*, 1969; *Fenner*, 1976]. High factor loadings are encountered for SSTsfeb below 0°C (Figure 4a) and for extensive sea-ice cover (Figure 5a). This assemblage is referred as an "Antarctic sea-sce zone" assemblage. It extends from the Weddell Sea to the Ross Sea around the Antarctic Continent (Figure 6).

Factor 2 accounts for 39.9% of the total variance with negative factor loadings (Table 4). It is dominated by *Fragilariopsis kerguelensis* and *Thalassiosira lentiginosa* (Table 5). High negative factor loadings fall between 2°C and 10°C for SSTsfeb (Figure 4b) and between 0 and 2 months of sea-ice cover per year (Figure 5b). This assemblage is referred as an "Antarctic open-ocean" assemblage and extends as a circumpolar belt constrained by the Subantacrtic front (SAF) to the north and minimum winter sea-ice edge to the south (Figure 6). It defines the well-preserved diatom-ooze surface belt described by *Burckle* [1984].

Factor 3 accounts for 8.3% of the total variance (Table 4) and is dominated by the *Chaetoceros* resting spores group (Table 5). High factor loadings are encountered for SSTfeb between 0°C and 2°C (Figure 4c) and for sea-ice cover between 5 and 9 months per year (Figure 5c). It is located around the Antarctic Peninsula and represents a "water stratification" assemblage (Figure 6). *Crosta et al.* [1997] showed that Antarctic *Chaetoceros* resting spores are preferentially encountered in neritic environments, particuliarly in the Antarctic Peninsula sector, and are indicators of a highly stratified surface water layer in relation to meltwater input. In deep-sea sediments they can be used as tracers of iceberg meltings. Although not indentifiable to species level because of the lack of morphological criteria, this group can be useful for paleoreconstructions.

Factor 4 accounts for 3.3% of the total variance (Table 4). It is dominated by five Subantarctic species *Thalassionema nitzschioides* var. *parva*, *Roperia tessalata*, *Thalassiosira oestrupii*, *Hemidiscus cuneiformis* and *Fragilariopsis doliolus* (Table 5). High factor loadings are encountered for SSTsfeb > 10°C (Figure 4d) and for no sea-ice cover throughout the year (Figure 5d). This assemblage is found north of the SAF in the Indian Ocean (Figure 6) and represents a "Subantarctic" assemblage.

3.1.2. IKM: Quantitative reconstruction of the modern model. Following *Imbrie and Kipp* [1971], we used a multiple curvilinear regression to quantify the relationships between the four floral factors in each of the 195 surface

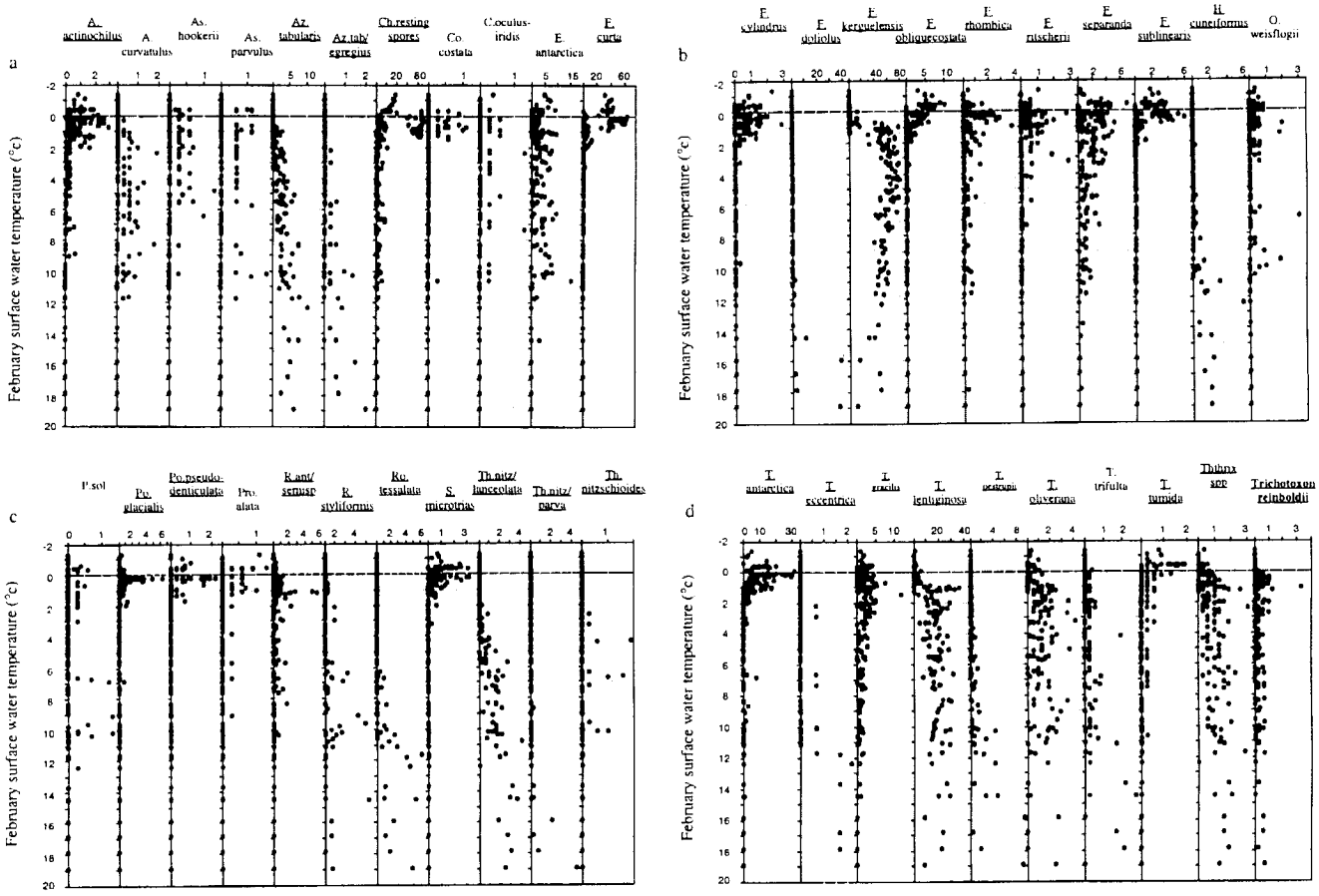

Figure 2. Relative abundances of 42 diatom taxa or taxa groups plotted against February sea surface temperatures: (a) from *Actinocyclus actinochilus* to *Fragilariopsis curta*, (b) from *Fragilariopsis cylindrus* to *Odontella weissflogii*, (c) from *Paralia sol* to *Thalassionema nitzschioides*, and (d) from *Thalassiosira antarctica* to *Trichotoxon reinboldii*. Species used in the diatom database are underlined.

sample sediments and the modern SSTsfeb and sea-ice cover. Estimated SSTsfeb are plotted against observed SSTsfeb in Figure 7a (open squares). The multiple correlation coefficient (MCC) is 0.97, and the slope of the correlation is 0.94. The mean of the residuals is 0.73°C. This value is lower than the standard deviation of the estimates (SEE) given by the equation (1.1°C) (Table 6). IKM195/33/4 accurately reconstructs SSTsfeb on the whole range of SSTs encountered in the Southern Ocean.

Estimated sea-ice cover values are plotted against observed values in Figure 7b (open squares). The MCC is 0.98, and the slope of the correlation line is 0.99. Mean residuals is 0.6 months of sea-ice presence per year (Table 6). This value is less than the SEE given by the equation (0.9 months of ice presence per year) (Table 6). The SEE is within the same range as the interannual variability of the sea-ice cover, showing that IKM195/33/4 accurately reconstructs this parameter. However, a striking feature is the negative estimates of sea-ice presence given by IKM195/33/4 (Figure 7b); modern sea-ice estimates can therefore be out of the range of the modern values.

3.1.3. MAT: Quantitative reconstruction of the modern model. Reconstruction of the modern model with the MAT approach has been tested for several parameters such as February and August SSTs, sea surface salinities, sea-ice extent and concentration, and finally, sea-ice presence in number of months per year. Only the results of SSTsfeb and sea-ice presence parameters are presented here. We will refer to this version of the transfer function in the future under the name of MAT$_5$195/33.

Estimated SSTsfeb are plotted against observed SSTsfeb in Figure 7a (solid circles). A simple linear regression between estimates and modern values displays a correlation coefficient of 0.96 and a slope of 0.89. Estimates are in a good agreement with the modern values to 10°C. Above this value, temperatures are underestimated because modern analogs are missing in the Subantarctic zone (SAZ). Residuals and SEE are good (mean residuals = 0.7°C, and mean SEE = 0.9°C) (Table 6). These results will be improved by the addition of new reliable surface sediment samples from the SAZ.

Estimated values of sea-ice cover are plotted against observed values in Figure 7b (solid circles). Both the correlation coefficient and the slope of the regression line are around 0.99, showing a good agreement of the estimates on the total range of modern sea-ice cover values (0-10 months of sea-ice presence per year). Mean residuals and mean SEE (0.3

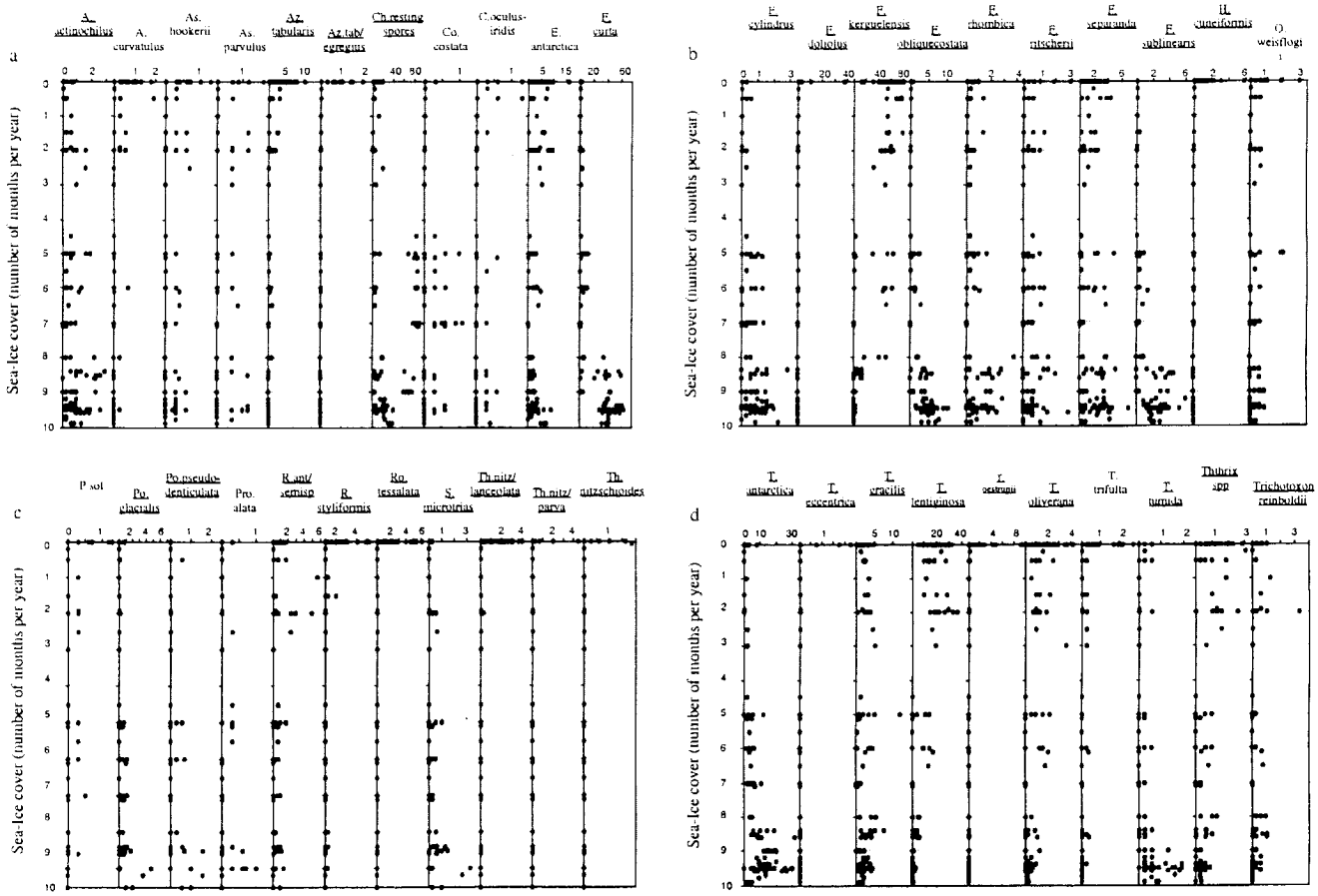

Figure 3. Relative abundances of 42 diatom taxa or taxa groups plotted against sea-ice cover: (a) from *Actinocyclus actinochilus* to *Fragilariopsis curta*, (b) from *Fragilariopsis cylindrus* to *Odontella weissflogii*, (c) from *Paralia sol* to *Thalassionema nitzschioides*, and (d) from *Thalassiosira antarctica* to *Trichotoxon reinboldii*. Species used in the diatom database are underlined.

and 0.4 month per year respectively) are very low in comparison to the annual variability of Antarctic sea-ice extent (Table 6). The MAT approach provides better results than the IKM approach for this parameter (no negative estimates and lower mean residuals and standard deviation). We therefore chose to use the MAT5195/33 for sea-ice paleoreconstructions.

3.2. Quantitative Reconstruction of the LGM Sea-Ice Presence

The MAT technique has been applied to 106 samples from the LGM dated around 18,000 years ago (Figure 8 and Table 2). Of those, 89 are CLIMAP points [*CLIMAP*, 1976, 1981] and the 17 others are from R/V *Marion Dufresnes* cruises. The same parameters have been reconstructed in the past using the MAT approach. Only results concerning sea-ice cover in number of months per year are presented here.

Table 4. Results of the *Q*-Mode Factor Analysis: A Focus on the Variance and the Cumulative Variance

	Factor 1	Factor 2	Factor 3	Factor 4
Variance	35.533	39.912	8.26	3.265
Cumulate Variance	35.533	75.444	83.705	86.969

The maximum extent of Southern Ocean sea ice at the LGM is inferred from the quantitative estimates of sea-ice presence provided by MAT5195/33 (Figure 8). This limit has been drawn north of control points displaying sea-ice presence greater than 0.5 month per year. However, some control points do not enter the general pattern of LGM sea-ice distribution and are not taken into account for the reconstruction of this limit (Figure 9). For example, the value of 1.1 months of sea-ice presence at 40°S in the western Indian sector of the Southern Ocean and very low sea-ice presence (0-0.8 months per year) around 60°S and 90°-110°E are thought to show advection, focusing, or dissolution phenomena. The LGM sea-ice limit (bold line) was more than 5° father north than its present position (thin line) (Figure 9). The maximum difference between the LGM and the present maximum sea-ice extent can be seen in the Atlantic sector of the Southern Ocean where winter sea-ice was around 8° north of today's limit. In this region the presence of the sea ice reached 3-5 months per year where nearly no sea-ice is present today. It confirms a greater expansion of sea ice at the LGM in the Atlantic sector.

Table 5. Varimax Factor Scores Matrix

Taxa/Factor	Factor 1	Factor 2	FActor 3	Factor 4
Actinocyclus actinochilus	0.239	0.004	0.04	-0.093
Azpetia tabularis	-0.105	-0.357	-0.009	0.137
Azpetia tab. var egregius	-0.016	-0.033	0.001	0.165
Chaetoceros resting spore gp.	0.165	-0.087	0.725	0.196
Fragilariopsis curta	0.444	0.1	0.157	-0.025
Fragilariopsis cylindrus	0.178	0.051	0.094	-0.009
Fragilariopsis doliolus	-0.007	-0.021	-0.023	0.279
Fragilariopsis kerguelensis	0.05	-0.531	0.1	-0.132
Fragilariopsis obliquecostata	0.367	0.076	-0.161	0.094
Fragilariopsis rhombica	0.238	-0.018	-0.245	0.065
Fragilariopsis ritscherii	0.132	-0.035	-0.005	-0.19
Fragilariopsis separanda	0.253	-0.21	-0.189	-0.071
Fragilariopsis sublinearis	0.355	0.085	-0.28	0.159
Hemidiscus cuneiformis	-0.009	-0.033	-0.036	0.298
Porosira glacialis	0.142	0.045	0.05	0.02
Porosira pseudodenticulata	0.152	0.035	-0.153	0.078
Rhizosolenia ant. var semis.	0.033	-0.083	0.104	-0.238
Rhizosolenia styliformis	-0.033	-0.057	0.054	0.167
Roperia tessalata	-0.012	-0.039	-0.035	0.359
Stellarima microtrias	0.249	0.065	-0.103	0.073
Thalassionama nitz. var lanc.	-0.062	-0.161	-0.014	0.439
Thalassionama nitz. var parva	-0.001	-0.005	-0.014	0.132
Thalassionema nitzschioides	-0.014	-0.022	0.021	0.022
Thalassiosira antarctica gp.	0.27	0.07	0.365	0.082
Thalassiosira eccentrica	-0.005	-0.015	-0.013	0.174
Thalassiosira gracilis	0.218	-0.242	0.072	-0.172
Thalassiosira lentiginosa	0.088	-0.427	-0.096	-0.006
Thalassiosira oestrupii	-0.04	-0.104	-0.011	0.327
Thalassiosira oest. var vanr.	0	-0.001	-0.005	0.06
Thalassiosira oliverana	0.022	-0.327	-0.097	-0.112
Thalassiosira tumida	0.172	0.016	-0.111	0.061
Thalassiothrix spp.	0.04	-0.287	-0.067	0.061
Trichotoxon reinboldii	0.012	-0.132	-0.011	-0.098

The position of winter sea ice during the LGM in the Pacific sector of the Southern Ocean cannot be determined with precision because we have too few LGM samples in this sector.

4. Discussion

4.1. Modern Model

IKM195/33/4 resolves four factors displaying 87% of the total variance (Table 4). The third factor represents a water stratification assemblage dominated by the *Chaetoceros* resting spores group (Table 5). This factor is located in the Gerlache and Bransfield Straits in the western part of the Antarctic Peninsula (Figure 6) where monogeneric assemblages of Chaetoceros resting spores are found in modern sediments. This region experiences important spring and summer blooms of Chaetoceros species [*Krebs*, 1983; *Leventer*, 1991] because of favorable growth conditions for this genus. Such conditions are a function of both low-salinity meltwater and protection from storm activity, both of which contribute to water column stability [*Amos*, 1987; *Huntley et al.*, 1987; *Leventer et al.*, 1993]. We chose to use the *Chaetoceros* resting spore group in our diatom database because very high relative percentages (>80%) of this group (Figures 2a and 3a) and high factor loadings (Figures 4c and 5c) constrain particular surface water conditions (-1°-1°C, and 5-8 months of sea ice per year). High factor loadings of this assemblage (ruled by high relative percentages of Chaetoceros resting spores) in fossil deep-sea sediments, where very few resting spores are generally found in surface sediment, are therefore indicators of water stratification due to iceberg melting [*Crosta et al.*, 1997]. Even if *Chaetoceros* resting spores represent a group of species of which little is known, their introduction in the diatom database is important to tracking iceberg melting and to trying to discriminate between sea-ice and iceberg paleoenvironnements, which had been already attempted with other diatom species by *Labeyrie et al.* [1986].

Reconstructions of the modern model of SSTsfeb and sea-ice cover using the new modern database have been tested by two statistical methods (IKM and MAT). Both methods are reliable approaches to reconstructing the two surface parameters even if SSTsfeb values above 12°C are underestimated with MAT5195/33 because of the lack of Subantarctic surface sediment samples (Table 6 and Figure 7a). In this case, IKM195/33/4 gives better results for high temperatures than MAT5195/33, which is more sensitive to the modern analog distribution as shown by *Prell* [1985]. For sea-ice cover reconstructions the lack of modern analogs in the SAZ is not so important because all these samples are in a zone of no sea-ice throughout the year. In this case, MAT5195/33 displays better estimates than IKM195/33/4 (Table 6 and Figure 7b). Moreover, MAT5195/33 does not present any negative estimates of sea-ice cover which are spurious in IKM195/33/4 results. We can therefore wonder if the IKM approach does not also provide nondiscernible erroneous SSTsfeb estimates. Because of these results and the relatively good distribution of the 195 surface sediment samples composing the modern database, we have chosen to use MAT15195/33 rather than IKM195/33/4 for paleoreconstructions of sea-ice conditions.

4.2. LGM Sea-Ice

MAT5195/33 allows us to reconstruct quantitatively LGM sea-ice presence per year and to draw the maximum sea-ice extent at this time. This limit, based on diatom analysis and statistical reconstruction, is compared to previous winter sea-ice estimations extrapolated from lithological boundaries, inferred sea-ice-rafted debris records, and faunal changes from deep-sea cores in Figure 8 [*Hays et al.*, 1976; *CLIMAP*, 1981; *Cooke and Hays*, 1982]. Despite using the same proxies and partially the same LGM data set, results given by these authors show large discrepancies (maximum of 5° of latitude in the Atlantic and the West Indian sectors of the Southen Ocean). Our maximum sea-ice limit (Figure 8, bold line) is in the variability of the former results despite using a totally different technique. Our results are in good agreement with *CLIMAP* [1981] results (Figure 8, thin line). However, discrepancies exist in two regions. The first one is located north of the Weddell Sea around 45°-50°S and 10°-50°W. We estimate there a greater winter sea-ice extension of 5° farther north than *CLIMAP* [1981]. MAT5195/33 provides quantitative estimates of 3-5 months of ice presence where nearly no sea ice is present today. *Hays et al.* [1976] and *Cooke and Hays* [1982] also find a greater winter sea-ice extension in this region than *CLIMAP* [1981] does, confirming our results. The second region is located in the eastern Pacific Ocean around 55°-60°S and 90°-120°W. Using

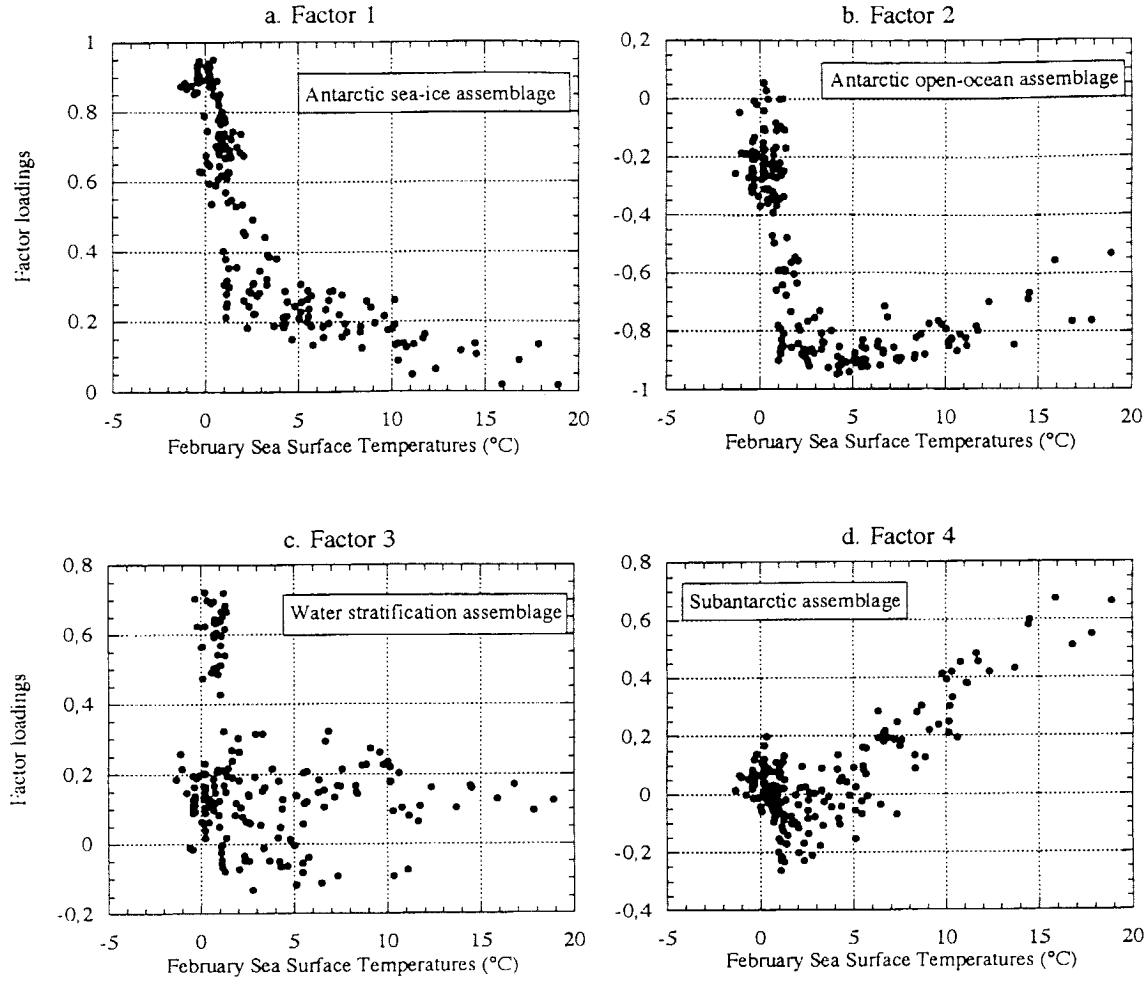

Figure 4. Factor loadings of the four factors resolved by IKM195/33/4 plotted against February sea surface temperatures.

the sedimentary parameters observed throughout the Antarctic Ocean (lithologic changes and sedimentation rate changes) and the relative position with respect to summer sea ice in the Atlantic and southwest Indian sectors 18,000 years ago, previous authors have mapped the winter sea-ice extent in the southeast Indian and Pacific Oceans at about 5° north of the summer sea-ice limit without any reliable control point. Despite having few samples in these sectors we present here a more reliable estimation of winter sea-ice cover in the southeast Indian and Pacific Oceans at the LGM. We think that the real winter sea-ice limit may be south of the limit given by *CLIMAP* [1981] (Figure 8). Quantitative estimates in this region are very low (around 0.5 months of sea-ice presence per year) (Figure 9), showing an important summer sea-ice meltback.

Antarctic sea ice is a highly variable feature of the Earth's surface and is known to play an important role in global climate. Sea ice interacts with both the atmosphere above and the ocean underneath in high latitudes [*Wu et al.*, 1997]. At its maximum extent in August/September, modern sea ice covers around 8% of the southern hemisphere (20 millions of square kilometers), about 1.5 times the area of the Antarctic itself (Figure 9, thin line). On Figure 9 the bold line represents the maximum extent of sea-ice 18,000 years ago estimated by MAT$_5$195/33. The LGM winter sea ice limit was located at least 5° north of its actual position. In the Atlantic sector of the Antarctic Ocean this limit was even near 8° farther north than today. The surface occupied by sea ice was around the double of the actual surface. Today, Antarctic sea-ice variations modify the westerlies which, in turn, affect the cyclonic behavior [*Simmonds and Jacka*, 1995]. More extensive sea-ice at the LGM may have lead to a greater cyclogenesis [*Simmonds*, 1996], and the zone of intense cyclogenesis may have been located farther to the north. These extratropical cyclones associated with the sea-ice edge may have transported moisture both to the southern midlatitudes leading to "cold outbreak" events [*Perrin and Simmonds*, 1995] and to the Antarctic ice cap. On the other hand the greater LGM sea-ice cap may have acted as an insulator between the warm ocean and the cold overlying air. This sheet prevented heat and moisture from reaching the lower atmospheric layers, leading to reduced precipitations over Antarctica as shown by the accumulation rate record of Vostok [*Jouzel et al.* 1987]. It also reduced the amount of solar radiation absorbed at the surface of the Earth.

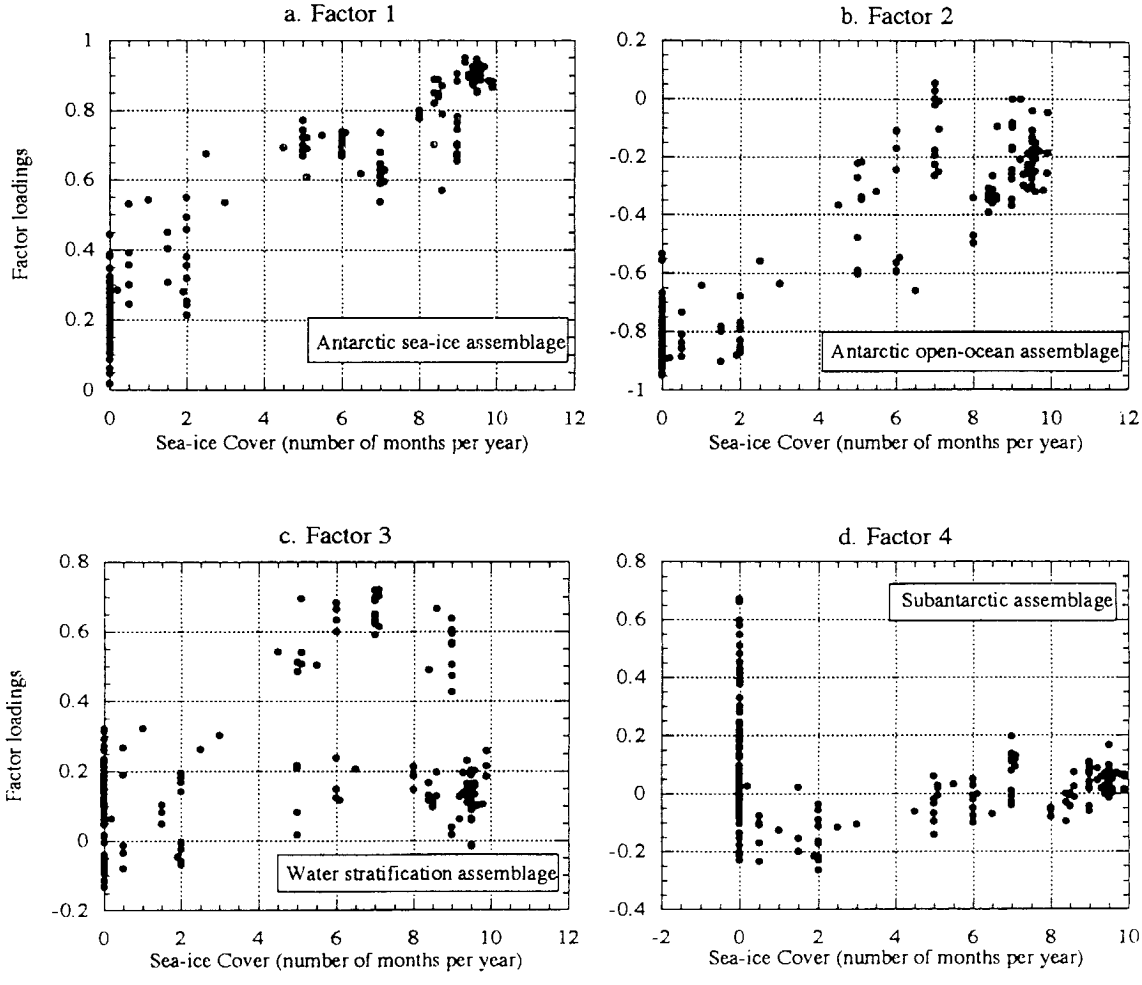

Figure 5. Factor loadings of the four factors resolved by IKM195/33/4 plotted against sea-ice cover.

This may greatly increase atmospheric cooling over the Antarctic Ocean, increasing the thermal gradient to the equator, and consequently, increasing the vigor of the atmospheric and surface oceanic circulations [*CLIMAP*, 1976; *Labeyrie et al.*, 1986, 1996]. Variations of sea-ice extent and concentration therefore influence southern semisphere midlatitudes and high latitudes, but climate also influences sea-ice conditions.

Analyzing cleaned diatom microfossils in cores from the Atlantic and Indian sectors of the Southern Ocean, *François et al.* [1997, Figure 4c, p. 33] found a depletion of $\partial^{15}N$ south of 50°S at the LGM in comparison to today. *François et al.* related this depletion of $\partial^{15}N$ to a significant decrease in the vertical supply rate of nitrate to the euphotic zone and thus to an increase in the degree of stratification of the surface water column. This zone of depletion is in good agreement with the maximum sea-ice extent at this time. The greater sea-ice extent and longer sea-ice presence may have played a significant role in stabilizing the upper water column by insulating it from the wind action and by meltwater input during the ice decay. The greater sea-ice cover may have participated in the reduction of the CO_2 "leak" from ocean to atmosphere by increased surface-water stratification and hence to the lowering of atmospheric CO_2 concentration during the LGM recorded in Vostok [*Barnola et al.*, 1987].

This study must be considered as preliminary as only the maximum sea-ice extent is presented here. The winter and summer sea ice 18,000 years ago around Antarctica are critical to drawing further conclusions on Southern Ocean paleoceanography and paleoclimatology. The point now is to reevaluate the extension of the Antarctic summer sea ice during the LGM when solar irradiation was not very different from today [*CLIMAP*, 1981]. In this optic, quantitative estimates of sea-ice presence can be very useful for paleoenvironmental interpretations. Near the Antarctic continent in the Indian sector, $MAT_5195/33$ estimates 6 months of sea-ice presence per year, which is comparable with modern conditions in this region. Spring/summer meltback of the ice was therefore not very different than today, and the mean position of summer sea-ice may be just a bit north of its present summer position in this sector (around 62°-65°S). This limit is well south of the summer position given by *Cooke and Hays* [1982], who estimated the summer sea-ice limit to be around 55°S in the Southern Indian sector. These preliminary results have to be

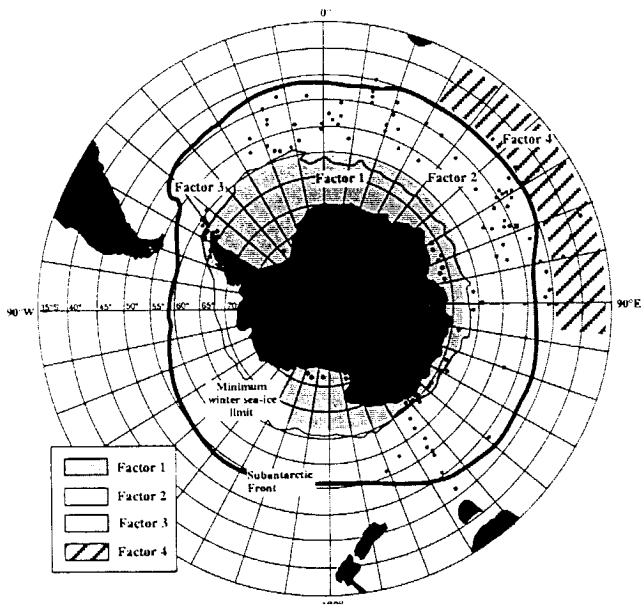

Figure 6. Distribution of the four factor resolved by IKM195/33/4 in modern Periantarctic sediments. The dots represent the positions of the 195 surface sediments used in the modern database. The location of the Subantarctic front is given according to *Tchernia* [1978] and of the minimal winter sea-ice extent is given according to the Naval Oceanography Command Detachment [1985].

improved in the future by the addition of new LGM samples more south and by the specific reconstruction of summer sea ice.

The MAT technique applied to Antarctic diatoms is a new approach for sea-ice paleoreconstruction. The advantage of MAT to lithological proxies is to provide numeric values of sea-ice cover which may be very important for reconstructions of the climate system via general circulation models.

Table 6. Reconstruction of the Modern Model by IKM195/33/4 and MAT5195/33

	IKM 195/33/4	MAT195/33/5
SSTsfeb		
R	0.97	0.96
MRES	0.73	0.7
MSEE	1.1	0.93
Sea-ice cover		
R	0.98	0.99
MRES	0.6	0.3
MSEE	0.9	0.4

SSTsfeb, February sea surface temperatures; R, correlation coefficient; MRES, mean of the residuals; and MSEE, mean of the standard errors.

5. Conclusions

1. Reconstruction of the modern model has been tested with two statistical techniques: IKM and MAT. MAT5195/33 gives better results on modern sea-ice models than IKM195/33/4. We have therefore chosen to use the MAT approach for sea-ice paleoreconstructions.

2. The application of MAT5195/33 to 106 periantarctic sediment samples dated around 18,000 years ago allow us to map the sea-ice cover at this time. The quantitative estimates confirm the winter sea-ice limit given by *CLIMAP* [1981] except in two regions of the Southern Ocean: in the Atlantic sector north of the Weddell Sea where MAT estimates more sea ice and in the eastern Pacific sector where MAT estimates less sea ice.

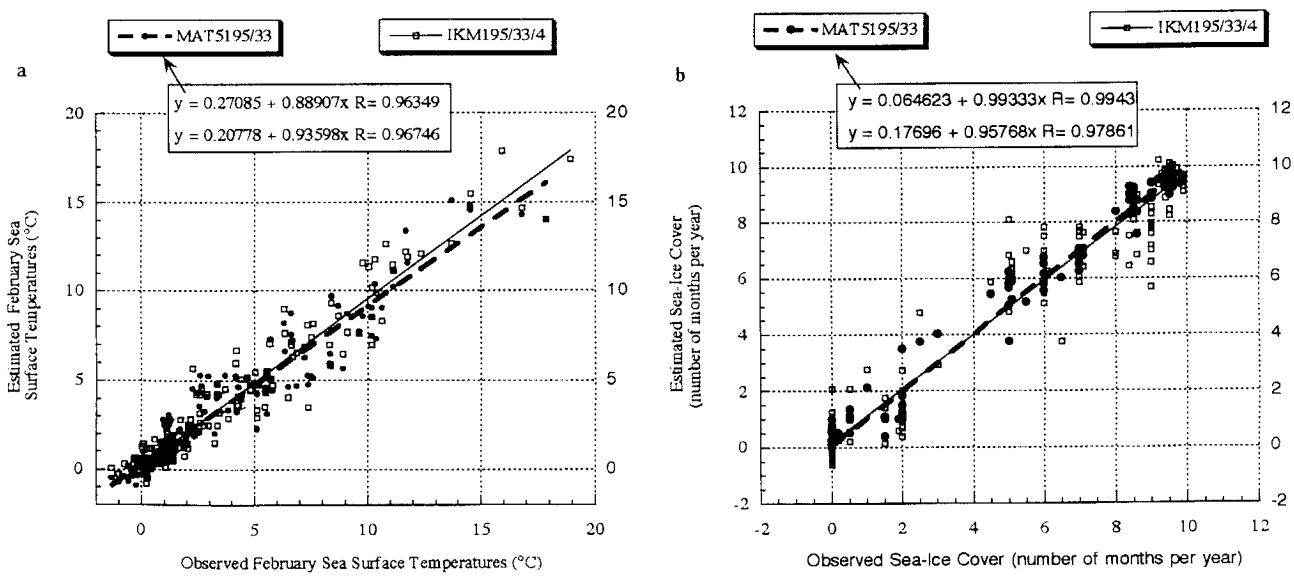

Figure 7. Observed values plotted against estimates for MAT5195/33 (solid circles) and IKM195/33/4 (open squares): (a) for February sea surface temperatures and (b) for sea-ice cover.

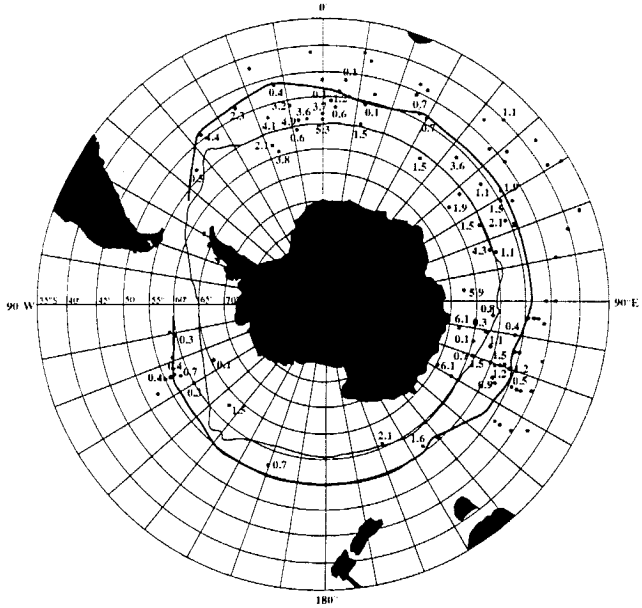

Figure 8. Maximum sea-ice extent at the last glacial maximum (LGM) estimated by MAT5195/33 (bold line) and from former authors such as Climate: Long-Range Investigation, Mapping, and prediction [*CLIMAP*, 1981] (thin line), *Hays et al.* [1976] (bold shaded line) and *Cooke and Hays* [1982] (thin dotted line). The dots represent the locations of the LGM samples used in this study.

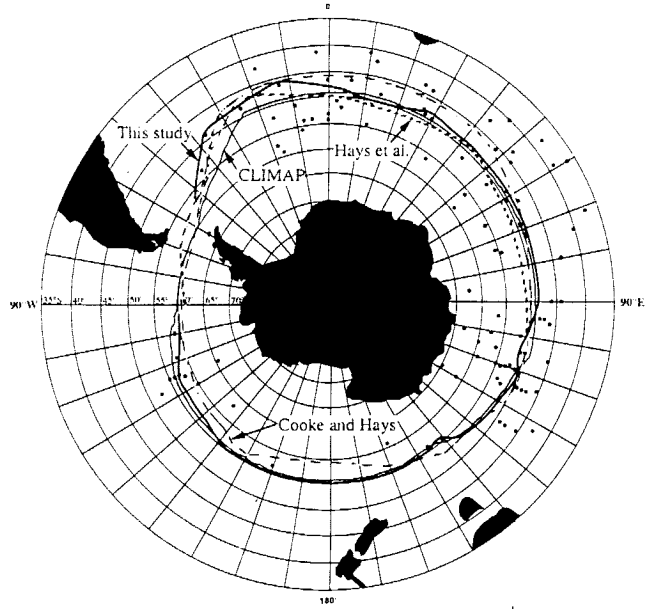

Figure 9. Modern (thin line) and last glacial maximum (bold line) maximum sea-ice extent. The dots represent the locations of the LGM samples used in this study. The estimated numerical values by MAT5195/33 represent LGM sea-ice presence in number of months per year. The dots with no associated value indicate no sea-ice presence throughout the year.

3. The greater sea-ice extent at the LGM may have been at the origin of a greater cyclogenesis. The cyclones may have an important effect on southern midlatitude and high-latitude climates. The greater sea-ice cover may also have reduced the amount of heat and moisture to the lower atmospheric layers.

4. The greater sea-ice cover may have participated in the lowering of atmospheric CO2 during the LGM and in reducing the leak of CO2 from the ocean to the atmosphere.

5. The mean position of the summer sea ice during the LGM may be south of the limit encountered in the literature. Additional work is necessary to determine this limit more accurately.

6. Quantitative estimates of sea-ice cover in number of months of ice presence are new paleoclimatic proxies that can be directly introduced in general circulation models to test or constrain the models.

Acknowledgments. We thank the LDEO Deep-Sea Sample Repository, which is funded by the National Science Fundation through grant OCE94-02150 and by the Office of Naval Research through grant N00014-96-I-0186, and the FSU core repository which kindly provided samples from the Robert Conrad, Vema, Island Orcadas and Eltanin cruises. We thank R. Gersonde, U. Zielinski, and L. Armand for our work on diatom taxonomy. We also thank U. Pflauman, N. Koç, P. Buat-Menard and M. Labracherie, and other anonymous referees for constructive reviews and comments on the manuscript. L.H. Burckle was funded by a grant/cooperative agreement from the National Oceanic and Atmospheric Administration (NOAA). The views expressed herein are those of the authors and do not necessarily reflect the views of NOAA or any of its subagencies. Financial support for this research was provided by CNRS (Centre National de la Recherche Scientifique), PNEDC (Programme National d'Etude de la Dynamique du Climat), and Missions Scientifiques des Terres Australes et Antarctiques Françaises (IFRTP-TAAF). This is DGO contribution 1215.

References

Amos, F.A., RACER: Physical oceanography of the western Bransfield Strait, *Antarc. J. U.S.*, *22*, 137-140, 1987.

Bareille, G., M. Labracherie, N. Maillet and C. Latouche, Quantification des teneurs en opale biogene des sediments de l'Ocean Austral par diffractometrie X, *Clay Miner.*, *25*, 363-373, 1990.

Barnola, J.M., D. Raynaud, Y.S. Korotkevich, and C. Lorius, Vostok ice core provides 160,000-year record of atmospheric CO_2, *Nature*, *329*, 408-414, 1987.

Burckle, L.H., Diatom distribution and paleoceanographic reconstruction in the Southern Ocean: Present and last glacial maximum, *Mar. Micropaleontol.*, *9*, 241-261, 1984.

Climate: Long-Range Investigation, Mapping, and Predictions (CLIMAP) Project Members, The surface of Ice-Age Earth: Quantitative geologic evidence is used to reconstruct boundary conditions for the climate 18,000 years ago, *Science*, *191*, 1131-1137, 1976.

Climate: Long-Range Investigation, Mapping, and Predictions (CLIMAP), Seasonal reconstructions of the Earth's surface at the last glacial maximum, *Geol. Soc. Am. Map Chart Ser., MC-36*, 1981.

Cooke, D.W., and J.D. Hays, Estimates of Antarctic Ocean seasonal sea-ice cover during glacial intervals, in *Antarctic Geoscience*, edited by C. Craddock, pp. 1017-1025, Union of Wisc. Press, Madison, Wisconsin, 1982.

Crosta, X., J.J. Pichon, and M. Labracherie, Distribution of Chaetoceros resting spores in modern peri-Antarctic sediments, *Mar. Micropaleontol.*, *29*, 238-299, 1997.

Defelice, D.R., and S.W. Wise, Surface lithofacies, biofaces, and diatom diversity patterns as models for delineation of climatic change in the southeast Atlantic Ocean, *Mari. Micropaleontol.*, *6*, 29-70, 1981.

Fenner, J., H.J. Schrader, and H. Wienigk, Diatom phytoplankton studies in the southern Pacific Ocean, composition and correlation to the Antarctic Convergence and its paleoecological significance, edited by C.D. Hollister et al., *Initial Rep. Deep Sea Drill. Proj., 35*, 757-813, 1976.

François, R., M.A. Altabet, E.F. Yu, D.M. Sigman, M.P. Bacon, M. Frank, G. Bohrmann, G. Bareille, and L. Labeyrie, Contribution of Southern Ocean surface-water stratification to low atmospheric CO_2 concentrations during the last glacial period, *Nature, 389*, 929-935, 1997.

Gersonde, R., and G. Wefer, Sedimentation of biogenic siliceous particles in Antarctic waters from the Atlantic sector, *Mar. Micropaleontol., 11*, 311-332, 1987.

Godfred-Spenning, C.R., and I., Simmonds, An analysis of Antarctic sea-ice and extratropical cyclone associations, International Journal of Climatology, 16, 1315-1332. 1996.

Hasle, G.R., *An analysis of the Phytoplancton of the Pacific Southern Ocean: Abundance, Composition, and Distribution During the Brategg Expedition, 1947-1948, Universitetsforlaget, Oslo, 1969.*

Hays, J.D., J.A. Lozano, N. Shackleton, and G. Irving, Reconstruction of the Atlantic and western Indian Ocean sectors of the 18.000 BP Antarctic Ocean, in *Investigation of Late Quaternary Paleoceanography and Paleoclimatology*, edited by R.M. Cline and J.D. Hays, pp. 337-372, Geol. Soc. of Am., Boulder, Color., 1976.

Horner, R.A., Ecology of sea-ice biota, in *Sea-Ice Biota*, edited by R.A. Horner, pp. 83-104, CRC Press, Boca Raton, Fl., 1985.

Howard, W.R., and W.L. Prell, Late Quaternary surface circulation of the southern Indian Ocean and its relationship to orbital variations, *Paleoceanography, 7*, 79-117, 1992.

Huntley, M.E., P. Niiler, O. Holm-Hansen, and D.H. Karl, RACER: Dynamics of the Antarctic Peninsula coastal ecosystem. An overview, *Antarct. J. U.S., 22*, 165-166, 1987.

Hutson, W.H., The Agulhas current during the late Pleistocene: Analysis of modern faunal analogs, *Science, 207*, 64-66, 1980.

Imbrie, J., and N.G. Kipp, A new micropaleontological method for quantitative paleoclimatology: Application to a late Pleistocene Carribean core, in *The Late Cenozoïc Glacial Ages?*, edited by K.K. Turekian, pp. 71-181, Yale Univ. Press, New Haven, Conn., 1971.

Jouzel, J., C. Lorius, J.R. Petit, C. Genthon, N.I. Barkov, V.M. Kotlyakov, and V.M. Petrov, Vostok ice core: A continuous isotope temperature record over the last climatic cycle (160,000 years), *Nature, 329*, 403-408, 1987.

Krebs, W.N., Ecology of neritic marine diatoms, Arthur Harbor, Antarctica, *Micropaleontology, 29*, 267-297, 1983.

Labeyrie, L.D., J.J. Pichon, M. Labracherie, P. Ippolito, J. Duprat, and J.C. Duplessy, Melting history of Antarctica during the past 60.000 years, *Nature, 322*, 701-706, 1986.

Labeyrie, L.D., et al., Hydrographic changes of the Southern Ocean (southeast Indian sector) over the last 230 kyr, *Paleoceanography, 11*, 57-76, 1996.

Laws, R.A., Preparing strewn slides for quantitative microscopical analysis: A test using calibrated microspheres, *Micropaleontology, 29*, 60-65, 1983.

Le, J., Paleotemperature estimation methods: Sensitivity test on two western equatorial pacific cores, *Quat. Sci. Rev., 11*, 801-820, 1992.

Le, J., and N.J. Shackleton, Recontructing paleoenvironment by transfert function: Model evaluation with simulated data, *Mar. Micropaleontol., 24*, 187-199, 1994.

Ledford-Hoffman, P.A., D.J. DeMaster, and C.A. Nittrouer, Biogenic-silica accumulation in the Ross Sea and the importance of Antarctic continental-shelf deposits in the marine silica budget, *Geochim. Cosmochim. Acta, 50*, 2099-2110, 1986.

Leventer, A., Sediment trap diatom assemblages from the northern Antarctic Peninsula region, *Deep Sea Res., 38*, 1127-1143, 1991.

Leventer, A., Modern distribution of diatoms in sediments from the Georges V coast, Antarctica, *Mar. Micropaleontol., 19*, 315-332, 1992.

Leventer, A., R.B. Dunbar, and D.J. DeMaster, Diatom evidence for the Late Holocene climatic events in Granite Harbor, Antarctica, *Paleoceanography, 8*, 373-386, 1993.

Levitus, S., World Ocean Atlas., disc 1, *Objective: Analyzes Temperature Fields*, U.S. Dep. Comm., Washington, D.C., 1994.

McIntyre, A., W.F. Ruddiman, K. Karlin, and A.C. Mix, Surface water response of the equatorial Atlantic Ocean to orbital forcing, *Paleoceanography, 4*, 19-55, 1989.

Mix, A., W.F. Ruddiman, and A. McIntyre, Late Quaternary paleoceanography of the tropical Atlantic, 1, Spatial variability of annual mean sea surface temperatures, 0-20,000years B.P, *Paleoceanography, 1*, 43-66, 1986.

Naval Oceanography Command Detachment, *Sea-Ice Climatic Atlas*, vol. 1, *Antarctic, MS 39527-5000*, pp. 131, Natl. Space Technol. Lab., Asheville, N.L., 1985.

Perrin, G., and I., Simmonds, The origin and characteristics of cold air outbreaks over Melbourne. *Aust. Meteorol. Mag., 44*, 41-59, 1995.

Pflaumann, U., J. Duprat, C. Pujol, and L.D. Labeyrie, SIMMAX: A modern analog technique to deduce Atlantic sea surface temperatures from planktonic foraminefera in deep-sea sediments, *Paleoceanography, 11*, 15-35, 1996.

Pichon, J.J., M. Labracherie, L.D. Labeyrie, and J. Duprat, Transfer function between diatom assemblages and surface hydrology in the Southern Ocean, *Paleogeogr. Paleoclimatol. Paleoecol., 61*, 79-95, 1987.

Pichon, J.J., L.D. Labeyrie, G. Bareille, M. Labracherie, J. Duprat, and J. Jouzel, Surface water temperature changes in the high latitudes of the southern hemisphere over the last glacial-interglacial cycle. *Paleoceanography, 7*, 289-318. 1992a.

Pichon, J.J., G. Bareille, M. Labracherie. L.D. Labeyrie, A. Baudrimont, and J.L. Turon, Quantification of the biogenic silica dissolution in the Southern Ocean sediments, *Quat. Res., 37*, 361-378, 1992b.

Prell, W.L., The stability of low-latitude sea-surface temperatures: An evaluation of the CLIMAP reconstruction with emphasis on the positive SST anomalies, *Rep. TR 025*, pp. 1-60, U.S. Dep. of Energy, Washington, D.C., 1985.

Rathburn, A.E., J.J. Pichon, M.A. Ayress, and P. DeDeckker, Microfossil and stable isotope evidence for changes in late Holocene paleoproductivity and paleoceanograpic conditions in the Prydz Bay region of Antarctica, *Palaeogeogr. Palaeoclimatol., Palaeoecol., 131*, 485-510, 1997.

Sakshaug, E., and O. Holm-Hansen, Factors governing pelagic production in polar oceans, in *Marine Phytoplankton and Productivity*, edited by O. Holm-Hansen et al., pp. 1-18, Springer-Verlag, New York, 1984.

Schrader, H.J., and R. Gersonde, Diatoms and silicoflagellates, in *Micropaleontological Counting Methods and Techniques: An Exercise on an Eight Meters Section of the Lower Pliocene of Capo Rossello, Sicily*, edited by W. J. Zachariasse et al., pp. 129-176, Utrecht Micropaleontol. Bull., Utrecht, N.L., 1978.

Simmonds, I., Climatic role of southern hemisphere extratropical cyclones and their relationship with sea-ice, *Pap. Proc.R. Soc. Tasmania, 130*, 95-100, 1996.

Simmonds, I., and T.H. Jacka, Relationships between the interannual variability of Antarctic sea-ice and the Southern Oscillation, *J. Clim., 8*, 637-647, 1995.

Tchernia, P., Oceanographie regionale, in *Description Physique des Oceans et des Mers*, pp. 28-95, Ed. Ecole Nat. Sup. de Tech. Avancees, Paris, 1978.

Truesdale, R.S., and T.B. Kellogg, Ross Sea diatoms: Modern assemblage distributions and their relationship to ecologic, oceanographic and sedimentary conditions, *Mar. Micropaleontol., 4*, 13-31, 1979.

Von Bodungen, B., V.S. Smetacek, M.M. Tilzer, and B. Zeitzschel, Primary production and sedimentation during spring in the Antarctic Peninsula region, *Deep Sea Res., 33*, 177-194, 1985.

Watkins, A.B., and Simmonds, I., Sensitivity of numerical prognoses to Antarctic sea-ice distribution. *J. Geophys. Res., 100*, 22,681-22,696, 1995.

Wilson, D.L., W.O. Smith, and D.M. Nelson, Phytoplankton bloom dynamics of the western Ross Sea ice-edge, I, Primary productivity and species specific production, *Deep Sea Res., 33*, 1375-1387, 1986.

Wu, X., I. Simmonds, and W.F. Budd, Modeling of Antarctic sea-ice in a general circulation model, *J. Clim., 10*, 593-609, 1997.

Zielinski, U., and R. Gersonde, Diatom distribution in Southern Ocean surface sediments (Atlantic sector): Implications for paleoenvironmental reconstructions, *Mar. Micropaleontol., 129*, 213-250, 1997.

X. Crosta and J.-J. Pichon, Département de Géologie et Océanographie, UMR-CNRS 5805, Université de Bordeaux I, Avenue des Facultés, 33405 Talence Cedex, France. (e-mail: crosta@geocean.u-bordeaux.fr; pichon@geocean.u-bordeaux.fr)

L. H. Burckle, Lamont-Doherty Earth Observatory of Columbia University, Palisades, N.Y. 10964. (e-mail: burckle@ldeo.columbia. edu)

(Received October 22, 1997;
revised January 16, 1998;
accepted January 30, 1998.)